Journal of Power Sources 240 (2013) 606–611

Contents lists available at SciVerse ScienceDirect

Journal of Power Sources

journal homepage: www.elsevier.com/locate/jpowsour

Synthesis of high dispersed intermetallic Ag_4Sn/C and its enhanced oxygen reduction reaction activity

Yuanjun Lu [a], Nanlin Zhang [b], Li An [b], Xiang Li [a], Dingguo Xia [b,*]

[a] College of Environmental & Energy Engineering, Beijing University of Technology, Beijing 100124, China
[b] Key Laboratory of Theory and Technology of Advanced Battery Materials, College of Engineering, Peking University, Beijing 100871, China

HIGHLIGHTS

- We have firstly synthesized carbon support nanoscale Ag_4Sn intermetallic compound (Ag_4Sn/C).
- The electrocatalytic performance of Ag_4Sn/C towards oxygen reduction reaction is superior to Ag/C.
- Ag_4Sn/C shows methanol tolerance property and good stability under DMAFC condition.

ARTICLE INFO

Article history:
Received 13 February 2013
Received in revised form
17 April 2013
Accepted 9 May 2013
Available online 17 May 2013

Keywords:
Intermetallic catalyst
Silver–tin material
Alkaline fuel cell
Oxygen reduction reaction

ABSTRACT

Ag_4Sn/C catalyst is synthesized by a solution phase reduction method assisted with ultrasonic at 0 °C. The as-prepared catalyst is characterized by transmission electron microscopy (TEM), X-ray diffraction (XRD) and electrochemical measurements. The Ag_4Sn intermetallic electrocatalyst displays enhanced electrocatalytic activity towards oxygen reduction reaction (ORR) and good methanol-tolerant property in alkaline media. The ORR catalyzed by Ag_4Sn/C proceeds a four-electron pathway. The obtained results are important for the development of Ag-based catalysts in alkaline fuel cells.

1. Introduction

Direct methanol alkaline fuel cell (DMAFC) has attracted much attention in recent years due to low operating temperature, less corrosive environment, and more facile kinetics for oxygen reduction [1,2]. It has great application potential in electrical vehicles, portable energy supplies, power station and aerospace, etc. However, the large scale commercialization of DMAFC technology is still hindered by the high cost, scarce resources and intolerance to methanol crossover of Pt-based cathode catalysts [3]. As a result, some alternative catalysts based on non-platinum metals have been explored, including the use of transition metal [4,5], carbon based materials [6], metal oxides [7], metal nitrides [8], and transition metal doped conducting polymer [9,10] in terms of their high conductivity, low price and favorable performances. Among those options, the relatively inexpensive and abundant Ag is a top candidate for DMAFC. Yet the poor affinity between Ag and O_2, which leads to difficulty in breaking O–O bond, is the main reason for the relatively low catalytic activity of Ag when compares to Pt [11]. Therefore, it is highly desirable to explore novel Ag-based catalyst for the development of DMAFC.

In previous works, the monometallic Ag electrocatalysts with small particle size and special morphologies exhibited better catalytic activity than bulk Ag in alkaline media [12,13]. AgPd alloy [14], Ag/Mn_xO_y [15] and AgCo bimetallic [11] showed enhanced ORR performance, which could be explained by the ensemble effect or the bifunctional mechanism. Although some impressive progresses have been brought about silver based materials, to the best of our knowledge, there haven't any reports about the electrocatalytic activity of silver based intermetallic nanoparticles towards ORR, as well as tolerance towards small organic molecules in fuel cell applications.

Pt-based intermetallics have been widely investigated as catalysts in fuel cell due to their unique ordered structures, like PtBi [16], PtFe [17], PtNi [18], etc. Chanho Pak et al. reported Pd_3Sn

* Corresponding author. Tel.: +86 10 62767962; fax: +86 10 62768316.
E-mail address: dgxia@pku.edu.cn (D. Xia).

0378-7753/$ – see front matter © 2013 Elsevier B.V. All rights reserved.
http://dx.doi.org/10.1016/j.jpowsour.2013.05.015

intermetallic has enhanced catalytic performance compared to PdSn alloy [19]. The mechanism of enhanced catalytic performance could be attributed to the electronic interaction between Pd and Sn, which caused a combined effect of reducing oxygen binding energy of Pd, and increasing O_2 adsorption affinity. Herein, from the point of view for catalyst design, Ag_4Sn could be a highly potential candidate as effective fuel cell catalyst relative to monometallic Ag. Previous works showed that Ag_4Sn was prepared through high temperature polyol process using poly(vinyl pyrrolidone) as capping agent. The as-prepared Ag_4Sn suffered from particles agglomeration [20] and block adsorption in active site by capping agent, which could suppress catalytic activity.

In this work, we reported a novel carbon supported Ag_4Sn intermetallic catalyst prepared by a solution phase co-reduction method assisted with ultrasonic at 0 °C in the absence of capping agent. The as-synthesized Ag_4Sn particles with average size of approximate 5 nm are uniformly dispersed on carbon support. Compared to Ag/C, Ag_4Sn/C was shown to have superior ORR activity and enhanced stability properties. Furthermore, high methanol tolerance in alkaline solution also proved that Ag_4Sn/C is a good candidate catalyst for ORR in DMAFC application.

2. Experimental section

2.1. Preparation and characterization

Carbon supported Ag_4Sn nanoparticles were synthesized by one-pot reduction of Ag and Sn precursor in EG/isopropanol mixed solution in an ultrasonic cleaning bath (45 kHz). In a typical preparation process, 0.6 mmol stannous octanoate and 0.2 mmol silver nitrate ($AgNO_3$) were dissolved into a mixed solution of 100 ml isopropanol and 200 ml ethylene glycol (EG). Then, 50 ml EG solution which contained 0.0783 g Vulcan XC-72 was gently added to the mixed solution under vigorous stirring. After purged with nitrogen for 1 h at 0 °C, sodium borohydride ($NaBH_4$) aqueous solution (0.2 M, 80 ml) was dropwisely added into the reaction solution, and kept stirring for another 6 h at 0 °C under nitrogen atmosphere in an ultrasonic cleaning bath. The resulting solid was filtered and washed with copious ethanol for several times, then dried at 80 °C for 12 h. In order to evaluate the influence of reaction temperature on product composition, control sample was also synthesized by the same procedure at room temperature. And for comparison use in electrochemical measurement, Ag/C and Sn/C was also synthesized at 0 °C.

Crystal structure of the products was characterized by X-ray diffraction (XRD, Bruker D8 Advance, Cu Kα radiation), and the morphology was investigated by transmission electron microscopy (TEM, Tecnai F30). Surface status was determined by using XPS (AXIS-Ultra instrument from Kratos Analytical, Al Kα radiation, $h\nu = 1486.6$ eV). To compensate for the effects of surface charges, the binding energies were calibrated using the C 1*s* hydrocarbon peak at 284.80 eV. The amount of Ag and Sn were determined by inductively coupled plasma-atomic emission spectroscopy (ICP-AES, PROFILE SPEC, Leeman) and TG analysis (EXSTAR TG/DTA 7300). During thermogravimetric analysis, the samples were heated from room temperature to 600 °C at 5 °C min^{-1}, and the air flow was precisely controlled at 200 mL_{air} min^{-1}.

2.2. Electrochemical measurements

Electrochemical measurements were carried out by SP-240 potentiostat (Bio-Logic SAS, France). The glassy carbon rotating disk electrode (GC-RDE) modified with catalysts ink (geometrical area 0.1257 cm^2) was used as working electrode in a conventional three electrode cell. Hg/HgO and glassy carbon (GC) were used as reference and counter electrode, respectively. It should be noted that all electrochemical measurements were further calibrated with respect to reversible hydrogen electrode (RHE) in order to give a more straightforward view of the catalysts performance in alkaline fuel cell applications. Catalysts inks were prepared by a typical process. 4 mg catalysts were suspended 30 min in 1 ml isopropanol which contained 80 μl 0.5 wt% Nafion solutions. The 10 μl of the suspension was pipetted onto the GC-RDE substrate and then dried in ambient atmosphere. Cyclic voltammetry (CV) measurements were carried out in N_2 saturated 0.1 M KOH between 0.213 V and 1.513 V vs. RHE. Polarization tests were performed in 0.1 M KOH with constantly purged O_2 at a scan rate of 10 mV s^{-1} between 0.213 V and 0.913 V Chronoamperometry and methanol-tolerant tests were conducted at 0.713 V in O_2 saturated 0.1 M KOH solution. The electrochemical measurements were all conducted at room temperature, i.e., 25 ± 1 °C.

3. Results and discussion

Fig. 1a shows the X-ray diffraction (XRD) patterns of as-prepared carbon supported Ag_4Sn intermetallic, in which characteristic peaks of chemically ordered hexagonal structure Ag_4Sn can be observed (JCPDS No. 29-1151), in addition to the minor Ag phase and bump corresponding to carbon support. While the XRD peaks of the control sample prepared under room temperature are in good agreement with fcc Ag (JCPDS No. 65-2871), as shown in Fig. 1b. Although the high concentration of stannous octanoate was added during the synthesis, no obvious peaks corresponding to tin-related compounds can be observed in the X-ray pattern. This phenomenon might be explained by the competitive more facile adsorption of Ag on the carbon surface sites, and the difficulty in reducing of stannous octanoate to metallic Sn at room temperature. This result is also consistent with Gyenge's [21].

Fig. 2 shows the TEM images of Ag_4Sn/C and Ag/C nanoparticles with average particle size of 5 nm and 8 nm, respectively, which are obviously smaller than many previous reported Ag-based materials [11,22]. This could be attributed to the slow mass transfer rate resulted from the high viscosity of EG at low temperature. As a result, high dispersion ultra-fine intermetallic Ag_4Sn particles on carbon support could be one step obtained. It has been shown that the catalyst with high surface area can enhance the activity towards oxygen reduction reaction. Therefore, this synthesis route presented in this paper is very promising to prepare high dispersion ultra-fine intermetallic particles.

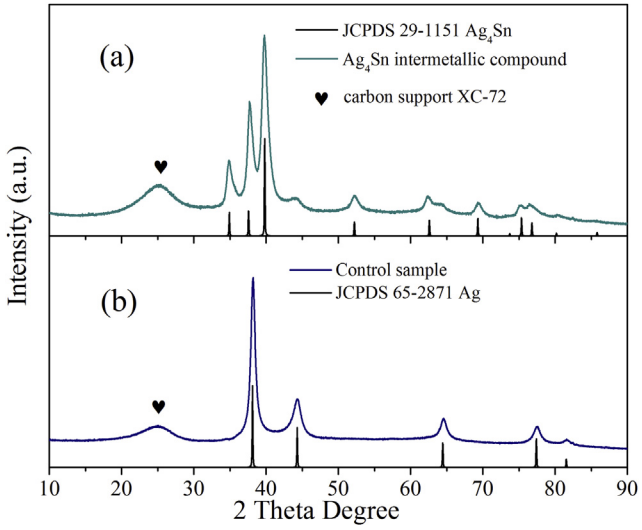

Fig. 1. XRD patterns of (a) carbon supported Ag_4Sn intermetallic compound prepared at 0 °C, and (b) control sample prepared under room temperature.

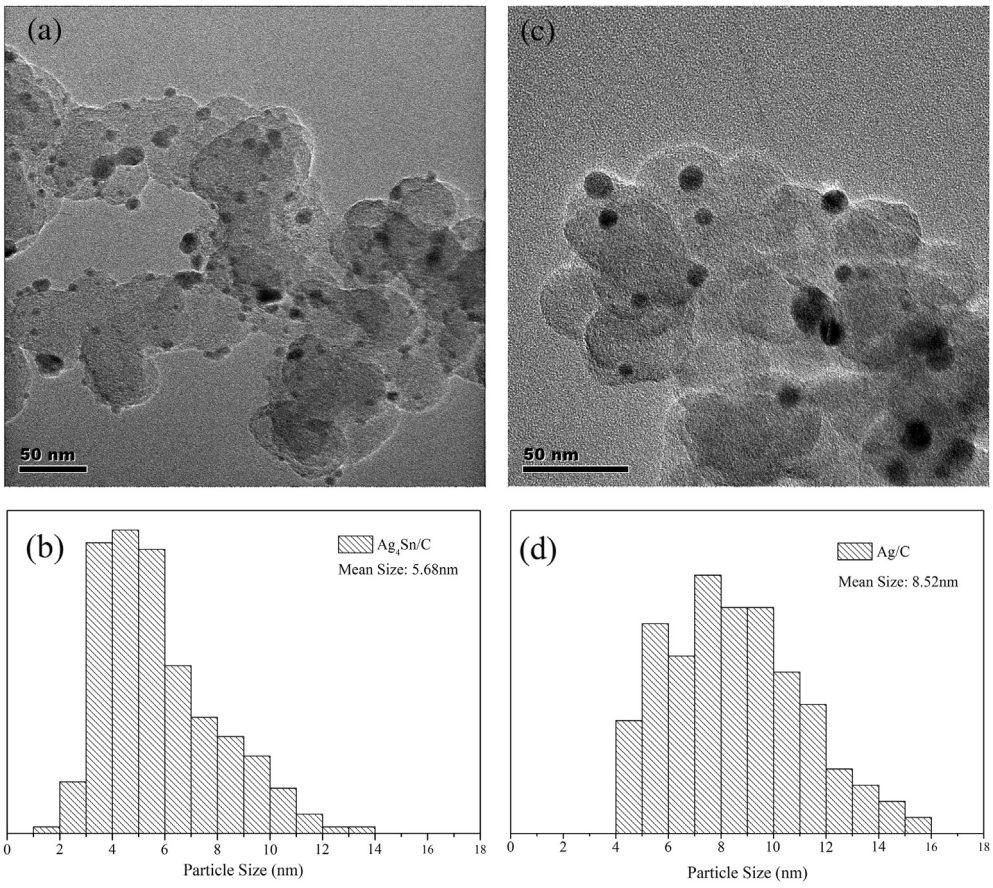

Fig. 2. TEM images and size distributions of Ag_4Sn/C (a), (b), and Ag/C (c), (d).

Chemical compositions of as-prepared catalysts were determined using inductively coupled plasma-atomic emission spectroscopy and TG analysis. Since Ag^+ could so easily react with trace amount of Cl^- ion in ICP-AES system that results in the deviation of chemical composition analysis, thereby in this work, only weight percentage of Sn was determined through ICP-AES to be 7% in Ag_4Sn/C, 27% in Sn/C respectively. Since the residue of Ag_4Sn/C sample after TG analysis was Ag and SnO_2 (determined by XRD, not shown here), therefore based on the following equation [23], $SnO_2(wt\%) = Sn(wt\%) \times$ (molecular weight of SnO_2/molecular weight of Sn) $\times$ 100, the weight percentage of Ag in Ag_4Sn/C and Ag/C were determined to be 21% and 20%, respectively, according to TG analysis [14].

The XPS spectrums of in Ag/C and Ag_4Sn/C are shown in Fig.3. The doublets in Fig. 3a are assigned to Sn $3d_{3/2}$ and $3d_{5/2}$ state of either SnO_2 or SnO at the surface of Ag_4Sn/C, since the binding energies of these two oxides are generally indistinguishable [21]. Fig. 3b presents XPS spectra of Ag 3*d* orbits. Virtually there are no obvious distinction of binding energy for Ag 3*d* orbits between Ag/C and Ag_4Sn/C (Ag $3d_{5/2}$ 368.65 eV and Ag $3d_{3/2}$ 374.65 eV), and both of which are in good agreement with 6 nm Ag nanoparticles supported on carbon (368.6 and 374.6 eV) [24], indicating the addition of Sn did not arouse obvious chemical shift of Ag. These results are consistent with Lee's work [25] and confirm the existence of Ag and Sn species on the surface of Ag_4Sn/C.

Fig. 4 presents the cyclic voltammogram (CV) of Ag/C and Ag_4Sn/C in N_2 saturated 0.1 M KOH electrolyte. Three anodic peaks (A_1, A_2, and A_3) and one cathodic peak are observed, and identified as described in the following sequence: the small peak A_1 was assigned to the simultaneous formation of a few monolayers of AgOH and soluble Ag(I) species, peak A_2 was associated with the formation of inner hydrous oxide layer, peak A_3 was related to the formation of more compact outer oxide layer, and the large reduction peak C_1 could be attributed to the electroreduction of the complex layer which formed during anodic reaction [26–28]. According to previous reports, the redox of SnO_2 or SnO does not occur within the same potential region [29], therefore it cannot be observed in the cyclic voltammogram in Fig. 3. It can be also seen that the oxidation peaks of Ag_4Sn/C have decreased, and especially, the oxidation process from Ag to AgOH or Ag_2O was inhibited so that peak A_1 was almost invisible. These results suggest that less Ag oxide species are formed during the anodic scanning. Moreover, the onset potential of C_1 for Ag_4Sn/C shifted to negative potential, indicating slightly more stable oxide formation. As to the reduction peak of silver oxide for Ag_4Sn/C shifted to positive potential, which seems to be contradiction with the negative shift of onset potential. We think it may result from the deviation of active material mass [30,31].

The kinetics of the ORR for Ag/C and Ag_4Sn/C catalyst were studied by the RDE method. Fig. 5a shows the ORR polarization curves of Ag_4Sn/C at different rotation rates. The Koutecky–Levich equation [27] was used to determine the electron transfer number of the catalyzed ORR.

$$1/J = 1/J_k + 1/J_L = 1/J_k + 1/\left(0.62nFD_o^{2/3}\nu^{-1/6}C_o\omega^{1/2}\right)$$

where J is the measured current density, J_k and J_L are the kinetic and limiting current density, respectively, n is the number of electron transferred, F is the Faraday constant (96,485 C mol^{-1}), C_O is the saturated concentration of O_2 in 0.1 M KOH (1.2×10^{-3} mol L^{-1}), D_o

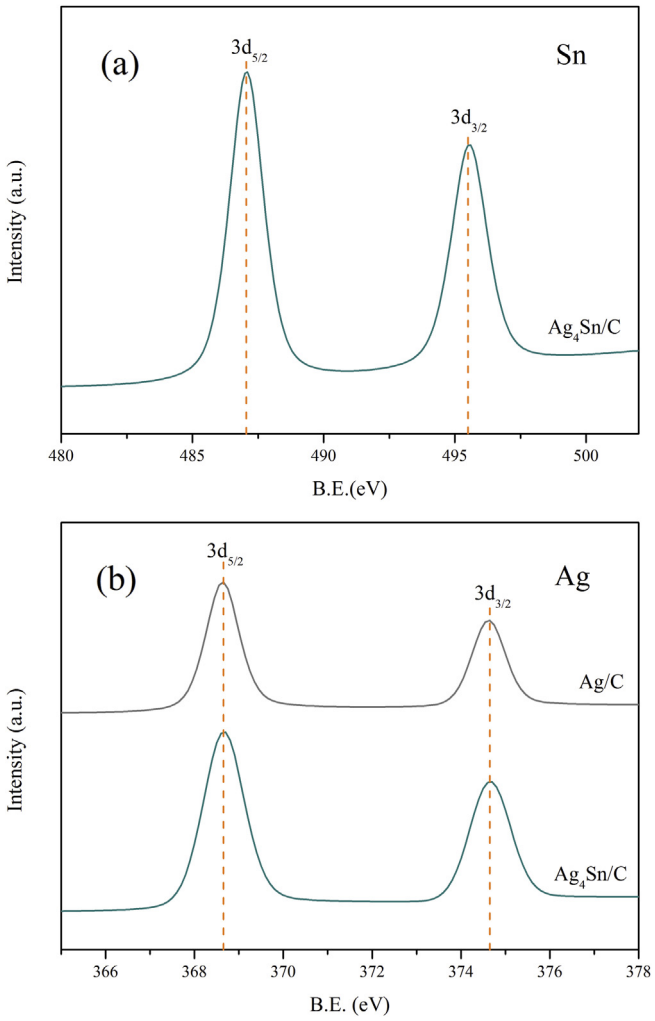

Fig. 3. XPS spectra of (a) Sn 3*d* in Ag_4Sn/C, (b) Ag 3*d* in Ag_4Sn/C and Ag/C.

is the diffusion coefficient of O_2 (1.9×10^{-5} cm^2 s^{-1}), ν is the kinetic viscosity of 0.1 M KOH (0.01 cm^2 s^{-1}), and ω is the electrode rotation rate. Fig. 5b is the K–L plots of Ag_4Sn/C at potential range from 0.51 V to 0.65 V, while the one for Ag/C is not shown here.

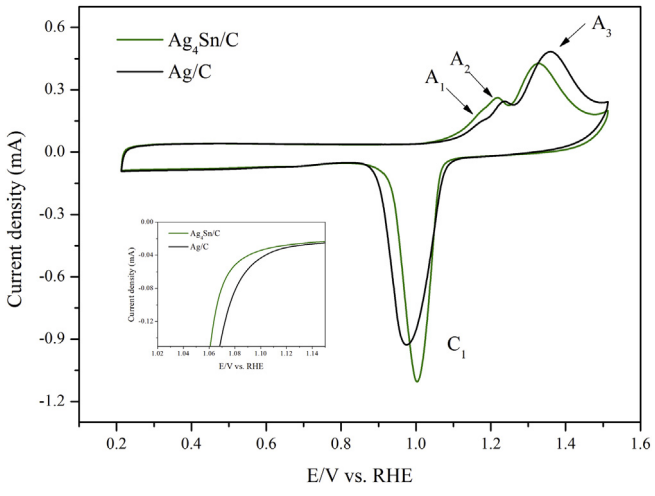

Fig. 4. Cyclic voltammograms of Ag/C and Ag_4Sn/C in N_2 saturated 0.1 M KOH solution at a scan rate of 50 mV s^{-1}, the inset is the magnification of peak C_1 onset.

According to the equation, *n* could be obtained by intercept of the Levich plots. And J_k is calculated on the basis of current density at 1600 rpm. It can be seen from Fig. 5b that the slopes of K–L plots for Ag_4Sn/C remain approximately constant over the potential range, which suggests a consistent electron transfer of ORR at different potentials. Additionally, the calculated numbers of electron transferred on both Ag/C and Ag_4Sn/C were close to 4, indicating a complete reduction of O_2 to OH^- on both catalysts. Meanwhile, Sn/C shows a very slow kinetic two-electron pathway of incomplete reducing O_2 to H_2O_2, as shown in Table 1.

Fig. 5c shows the ORR polarization curves for oxygen reduction on Ag/C, Sn/C and Ag_4Sn/C catalysts. The results were summarized in Table 1. The onset potential (E_{onset}) shifted to higher value for Ag_4Sn/C compare to Ag/C, and the kinetic mass activity at different potentials on Ag_4Sn/C was more than three times larger than Ag/C at 0.6 V, suggesting markedly improved dynamics for ORR relative to Ag/C catalyst. It is worth mentioning that kinetic current density and onset potential are two essential parameters that represent the kinetic and thermodynamic characteristics of the catalytic reaction. Compared with previous reports about Ag-based materials in fuel cell applications, Ag_4Sn/C shows a comparable oxygen reduction onset potential with silver-molybdate [22], Ag NPs@POM-CNTs [32] and silver–cobalt bimetallic [11] and much higher activity than AgMn [33] and AgCu [34]. Furthermore, the kinetic current density normalized by geometric area of the working electrode were also given in this work. The calculated results for kinetic current of Ag_4Sn/C were much higher than previous report of AgAu bimetallic [35], yet still lower than AgCo [11] bimetallic and $CoPcF_{16}$@Ag/C [36] composite which might due to the difference in catalyst loading, morphologies, and their use of gas diffusion electrode.

As to the origin of enhanced oxygen reduction activity of Ag_4Sn/C, it may be relevant to the surface species of Ag_4Sn/C nanoparticles, which are Ag and SnO (or SnO_2) confirmed by XPS analysis. Karen E. Swider-Lyons [29] reported higher onset potential of ORR for Au-SnO_x/VC in comparison with Au/VC electrocatalyst and referred this improvement to a bifunctional mechanism, in which O_2 is chemisorbed onto SnO surface in the form of O_2^-, and then further reduced on Au. In addition, this hypothesis was also used to explain the enhanced catalytic activity of SnO_2 supported Au [37]. Therefore, based on previous researches, such bifunctional mechanism could also be the origin of the enhanced activity of Ag_4Sn/C. The ORR process could be promoted with the existence of SnO since both Ag and Au are thermodynamically unfavorable to adsorb and split oxygen [38].

Methanol tolerance is a key characteristic for cathode materials in DMAFC applications, therefore it is necessary to examine the effect of methanol in ongoing ORR process. To examine the crossover effect, chronoamperometry measurement was employed for Ag_4Sn/C, and for comparison, Pt/C has also been tested by the same measurement, the results are shown in Fig. 6. Two arrows in both *i*–*t* curves imply the injection of 2 ml methanol into 100 ml O_2 saturated 0.1 M KOH electrolyte (i.e. the concentration of methanol was 0.5 M). For Ag_4Sn/C, the injection of methanol did not arouse an obvious oxidation curve, which indicates that Ag_4Sn/C is high tolerant towards methanol. Meanwhile, *i*–*t* curve of Pt/C showed a high responsive current corresponding to methanol oxidation, the current density was almost half of the beginning after the curve was stable again, indicating that methanol has a mixed potential effect on Pt/C catalysts [39].

Fig. 7 compares the chronoamperometry curves of Ag/C and Ag_4Sn/C. After operating the cell at 0.713 V for 24 h, relative current of Ag_4Sn/C drop to 88%, while Ag/C exhibits more obvious decrease with a current loss of approximately 73%, suggesting enhanced stability of Ag_4Sn/C intermetallic catalyst.

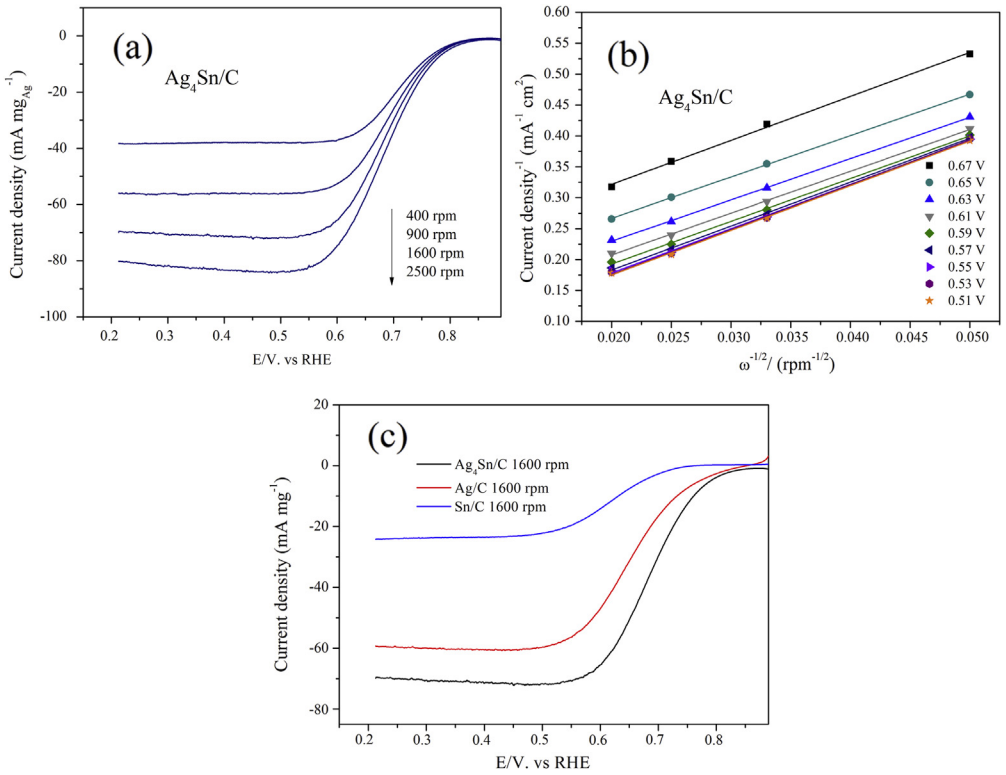

Fig. 5. (a) Polarization curves for the ORR in O_2 saturated 0.1 M KOH at different rotation rates on Ag_4Sn/C at a scan rate of 10 mV s^{-1}, (b) Koutecky–Levich plots for Ag_4Sn/C catalyst obtained at different potentials, (c) ORR polarization curves obtained on Ag_4Sn/C, Ag/C and Sn/C in 0.1 M KOH saturated with oxygen at 1600 rpm, scan rate: 10 mV s^{-1}.

Table 1
Parameters of ORR on Ag_4Sn/C, Ag/C and Sn/C catalysts.

Catalysts	E_{onset} vs. RHE	Kinetic current density (mA mg^{-1})/(mA cm^{-2}_{geo})				Number of electron transferred
		0.75 V	0.70 V	0.65 V	0.60 V	
Ag_4Sn/C	0.77	15.68/1.05	52.01/3.48	172.09/11.50	759.31/50.76	3.9
Ag/C	0.74	8.40/0.53	22.75/1.45	65.13/4.14	209.62/13.34	3.8
Sn/C	0.73	0.25/0.02	3.06/0.26	11.11/0.96	35.70/3.06	2.2

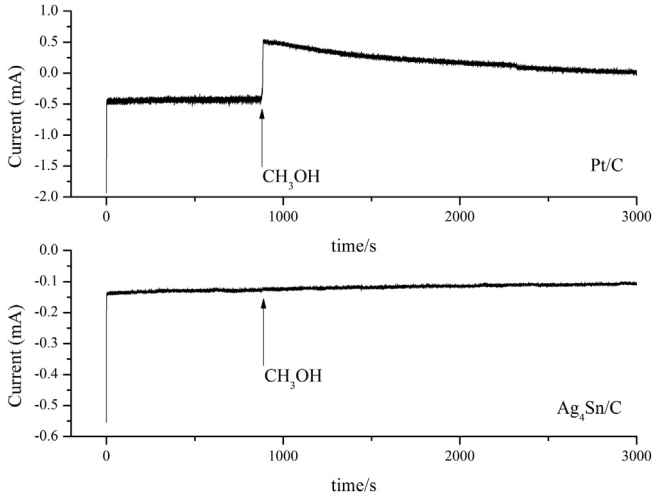

Fig. 6. Chronoamperometry curves of Pt/C and Ag_4Sn/C in O_2 saturated 0.1 M KOH under magnetic stirring (300 rpm), the applied potential was 0.713 V. Arrows indicate the addition of 0.5 M methanol into electrolyte.

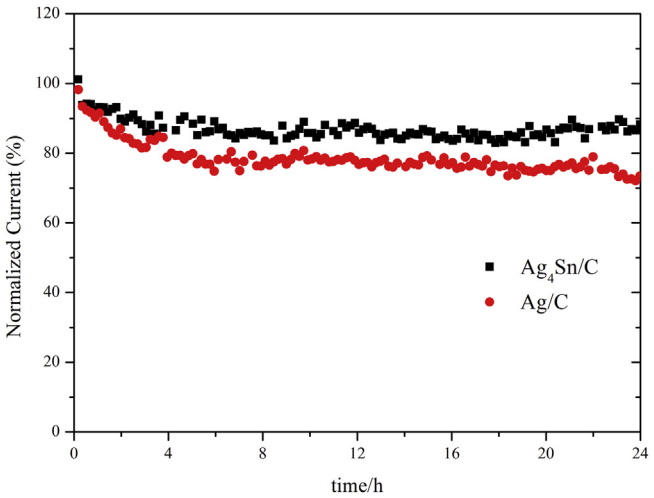

Fig. 7. Chronoamperometry curves of Ag/C and Ag_4Sn/C catalysts at electrode potential of 0.713 V in O_2 saturated 0.1 M KOH solution.

4. Conclusions

In summary, a novel Ag_4Sn/C intermetallic catalyst was synthesized by low temperature chemical reduction method assisted with ultrasonic. This method efficiently synchronized the reduction rate of different metal ionic, therefore ultra-fine and high dispersed intermetallic nanoparticles could be obtained by one step procedure. For the first time, nanoscale Ag_4Sn/C was used to catalyze ORR in DMAFC application, and showed enhanced catalytic activity. Furthermore, Ag_4Sn/C also showed high methanol tolerance and good long-term stability in alkaline media. Therefore, the low cost Ag_4Sn/C with facile synthesis route could be regarded as high potential catalyst for the ORR in DMAFC application.

Acknowledgements

The authors acknowledge the financial supports from the major program of Beijing Municipal Natural Science Foundation (No. 20110001), National Natural Science Foundation of China (No. 11179001), National High Technology Research and Development Program (863, No. 2012AA052201).

References

[1] Z.W. Chen, D. Higgins, A.P. Yu, L. Zhang, J.J. Zhang, Energy Environ. Sci. 4 (2011) 3167–3192.
[2] J.S. Spendelow, A. Wieckowski, Phys. Chem. Chem. Phys. 9 (2007) 2654–2675.
[3] A.S. Aricò, S. Srinivasan, V. Antonucci, Fuel Cells 1 (2001) 133–161.
[4] H.J. Yin, H.J. Wang, D. Wang, Y. Gao, Z.Y. Tang, ACS Nano 6 (2012) 8288–8297.
[5] J.J. Salvador-Pascual, S. Citalán-Cigarroa, O. Solorza-Feria, J. Power Sources 172 (2007) 229–234.
[6] K.P. Gong, F. Du, Z.H. Xia, M. Durstock, L.M. Dai, Science 323 (2009) 760–764.
[7] Z. Yang, X.M. Zhou, H.G. Nie, Z. Yao, S.M. Huang, ACS Appl. Mater. Interfaces 3 (2011) 2601–2606.
[8] D.G. Xia, S.Z. Liu, Z.Y. Wang, G. Chen, L.J. Zhang, L. Zhang, S.Q. Hui, J.J. Zhang, J. Power Sources 177 (2008) 296–302.
[9] X. Chen, F. Li, X.Y. Wang, S.R. Sun, D.G. Xia, J. Phys. Chem. C 116 (2012) 12553–12558.
[10] X. Chen, S.R. Sun, X.Y. Wang, F. Li, D.G. Xia, J. Phys. Chem. C 116 (2012) 22737–22742.
[11] F.H.B. Lima, J.F.R. de Castro, E.A. Ticianelli, J. Power Sources 161 (2006) 806–812.
[12] Y.Z. Lu, W. Chen, J. Power Sources 197 (2012) 107–110.
[13] N. Wang, X. Cao, Q.J. Chen, G. Lin, Chem. Eur. J. 18 (2012) 6049–6054.
[14] D.A. Slanac, W.G. Hardin, K.P. Johnston, K.J. Stevenson, J. Am. Chem. Soc. 134 (2012) 9812–9819.
[15] D.A. Slanac, A. Lie, J.A. Paulson, K.J. Stevenson, K.P. Johnston, J. Phys. Chem. C 116 (2012) 11032–11039.
[16] D.G. Xia, G. Chen, Z.Y. Wang, J.J. Zhang, S.Q. Hui, D. Ghosh, H.J. Wang, Chem. Mater. 18 (2006) 5746–5749.
[17] X. Li, L. An, X.Y. Wang, F. Li, R.Q. Zou, D.G. Xia, J. Mater. Chem. 22 (2012) 6047–6052.
[18] J. Greeley, I.E.L. Stephens, A.S. Bondarenko, T.P. Johansson, H.A. Hansen, T.F. Jaramillo, J. Rossmeisl, I. Chorkendorff, J.K. Nøskov, Nat. Chem. 1 (2009) 552–556.
[19] S.A. Jin, K. Kwon, C. Pak, H. Chang, Catal. Today 164 (2011) 176–180.
[20] R.E. Cable, R.E. Schaak, Chem. Mater. 17 (2005) 6835–6841.
[21] A. Ignaszak, C. Teo, S.Y. Ye, E. Gyenge, J. Phys. Chem. C 114 (2010) 16488–16504.
[22] Y. Wang, Y. Liu, X.J. Lu, Z.P. Li, H.N. Zhang, X.J. Cui, Y. Zhang, Electrochem. Commun. 20 (2012) 171–174.
[23] Y.H. Xu, J.C. Guo, C.S. Wang, J. Mater. Chem. 22 (2012) 9562–9567.
[24] I. Lopez-Salido, D.C. Lim, Y.D. Kim, Surf. Sci. 588 (2005) 6–18.
[25] Y.H. Jo, I. Jung, N.R. Kim, H.M. Lee, J. Nanopart. Res. 14 (2012) 782–791.
[26] M. Hepel, M. Tomkiewicz, J. Electrochem. Soc. 131 (1984) 1288–1294.
[27] Y.Z. Lu, Y.C. Wang, W. Chen, J. Power Sources 196 (2011) 3033–3038.
[28] S. Maheswari, P. Sridhar, S. Pitchumani, Electrocatalysis 3 (2012) 13–21.
[29] W.S. Baker, J.J. Pietron, M.E. Teliska, P.J. Bouwman, D.E. Ramaker, K.E. Swider-Lyons, J. Electrochem. Soc. 153 (2006) A1702–A1707.
[30] G. Wu, K.L. More, C.M. Johnston, P. Zelenay, Science 332 (2011) 443–447.
[31] J. Chlistunoff, J. Phys. Chem. C 115 (2011) 6496–6507.
[32] R.J. Liu, S.W. Li, X.L. Yu, G.J. Zhang, Y. Ma, J.N. Yao, J. Mater. Chem. 21 (2011) 14917–14924.
[33] M.A. Kostowskyj, D.W. Kirk, S.J. Thorpe, Int. J. Hydrogen Energy 35 (2010) 5666–5672.
[34] M. Han, S.L. Liu, L.Y. Zhang, C. Zhang, W.W. Tu, Z.H. Dai, J.C. Bao, ACS Appl. Mater. Interfaces 4 (2012) 6654–6660.
[35] Y. Song, K. Liu, S.W. Chen, Langmuir 28 (2012) 17,143–17,152.
[36] J.S. Guo, H.X. Li, H. He, D. Chu, R.R. Chen, J. Phys. Chem. C 115 (2011) 8494–8502.
[37] W. Chen, D. Ny, S.W. Chen, J. Power Sources 195 (2010) 412–418.
[38] J.L. Fernández, D.A. Walsh, A.J. Bard, J. Am. Chem. Soc. 127 (2005) 357–365.
[39] A. Rabis, P. Rodriguez, T.J. Schmidt, ACS Catal. 2 (2012) 864–890.